Deep Velocity Profiling Using Lowered Acoustic Doppler Current Profilers: Bottom Track and Inverse Solutions*

MARTIN VISBECK

Lamont-Doherty Earth Observatory, Columbia University, Palisades, New York

(Manuscript received 5 June 2000, in final form 15 October 2001)

ABSTRACT

Lowered acoustic Doppler current profilers (LADCPs) have matured from an experimental instrument to an operational hydrographic tool to study ocean dynamics. The data processing, however, is still in a rather primitive state. First, a method to estimate bottom-track velocities using the standard water profile data was developed. Then inverse solutions are presented that enhance the standard data processing by adding external constraints such as bottom-referenced velocity profiles. Depending on the depth of the profile and the ADCP range the inclusion of bottom-track data can reduce the local velocity errors by a significant factor. The least squares framework also allows for simplified error analysis of the LADCP system and some of the trade-offs are discussed.

1. Introduction

Direct velocity observations have allowed the study of many new aspects of ocean dynamics. For example the advent of vessel-mounted acoustic Doppler current profiler (VMADCP) (e.g., Joyce et al. 1982) has provided detailed insights into upper-ocean dynamics. However, the limited range to a maximum depth of 300 to possibly 800 m (with reduced accuracy) left much to be desired. One way to overcome this limitation is to lower one or two self-contained ADCPs together with hydrographic sensor packages [which we will refer to as a conductivity–temperature–depth (CTD) recorder], a method that has become known as LADCP profiling (see Firing 1998, for a recent review).

The first lowered ADCP (LADCP) cast was taken in 1989 at a site near Hawaii by Firing and Gordon (1990). They showed that useful information was contained in the data, but argued that the expected errors of the system might be too large ($\sim$10 cm s^{-1}) for many applications. A year later in 1990 Fischer and Visbeck (1993) used a similar system during a cruise in the tropical Atlantic. They had the advantage of simultaneous independent velocity profiles from a Pegasus system (Spain et al. 1981) that allowed them to carefully evaluate the LADCP performance. They concluded that if care was taken LADCPs were able to reproduce much of the velocity field in comparison to the more accurate Pegasus system.

In recent years LADCPs were used extensively throughout the World Ocean Circulation Experiment (WOCE) era (Firing 1998) and provided a wealth of useful top to bottom velocity profiles (e.g., Beal and Bryden 1997; Firing et al. 1998; Fischer et al. 1996; Hinrichsen and Lehmann 1995; Schott et al. 1993; Stramma et al. 1996; Wijffels et al. 1998; Wilson and Johns 1997).

The optimal choice of instrument hardware and parameter setting is still an open issue. Several factors have to be taken into account ranging from different acoustical properties of the ocean that themselves are a function of frequency, depth, and region; instrument design, large or small beam angle, and bandwidth. All of those parameters contribute to the more fundamental trade-off between range and accuracy. A better understanding of the LADCP system and error propagation will allow for optimal hardware and parameter choices.

More recently we have started to pay attention to the bottom-reflected data of the LADCP system. Wilson (1994) and King (1998, personal communication) were among the first to try the RDI built-in bottom-track mode and reported good bottom-tracked velocity profiles over a range of 50–250 m above the bottom even at water depths exceeding 3000 m. However, a fundamental questions arises: How can we optimally use this and/or other external information to improve the ocean velocity profile estimate?

In the following we briefly review the fundamentals of LADCP profiling (section 2) and discuss aspects of LADCP sampling (section 3). Different bottom-track

* Lamont-Doherty Earth Observatory Contribution Number 6279.

Corresponding author address: Dr. Martin Visbeck, Department of Earth and Environmental Sciences, Lamont-Doherty Earth Observatory, Columbia University, 61 Route 9W, Palisades, NY 10964-8000.
E-mail: visbeck@ldeo.columbia.edu

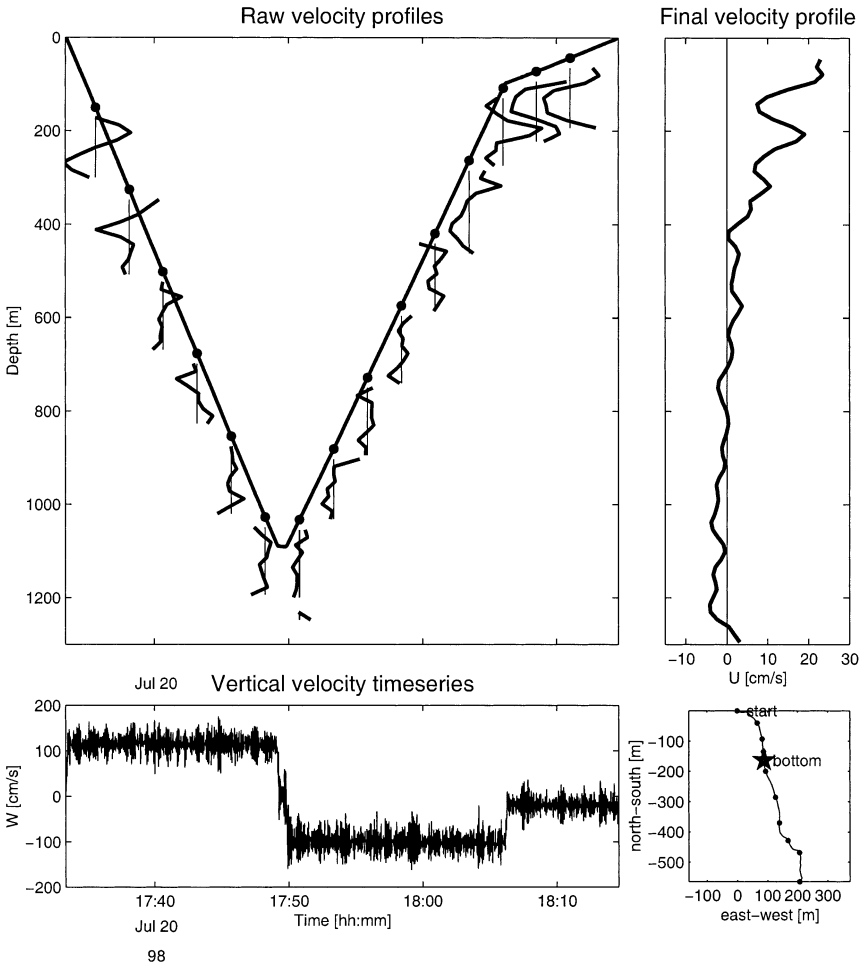

FIG. 1. LADCP velocity profiling. (top left) An idealized LADCP cast in the depth–time dimension. The solid line represents the CTD depth as a function of time descending from the surface to the bottom and back to the surface. The shorter thick lines are examples of individual ADCP profiles with an unknown CTD velocity removed. (bottom left) The raw vertical velocity of the package as a function of time. Note, that its time integral represents the depth of the package as shown in the top-left panel. (upper right) The estimated final ocean velocity profile of which small segments were observed by each individual ADCP profile. (bottom right) The relative position of the package in the *X*–*Y* frame. The position of the start and when the CTD was at its deepest point are marked.

modes are reviewed and a new method derived that allows one to obtain ''bottom-track velocities'' from the standard (non–bottom track) LADCP data (section 4). In section 5 the basics of an improved data processing scheme based on inverse methods are described. Its performance and advantages are discussed and summarized in section 6.

2. Fundamentals of LADCP profiling

The assumption behind the LADCP method is that one can use successive overlapping velocity profiles, which individually cover only a small fraction of the water column, to obtain a full ocean depth velocity profile (Fig. 1a). Each ADCP velocity observation can be interpreted as the sum of three parts:

$$U_{\text{adcp}} = U_{\text{ocean}} + U_{\text{ctd}} + U_{\text{noise}}. \quad (1)$$

Here U_{ctd} is the motion of the ADCP that is mounted on the CTD frame. A priori we know two aspects about U_{ctd}: the time integral over the whole cast (of duration T) is equal to the horizontal ship displacement during the cast (either due to drift or active motion) DX_{ship}:

$$\text{DX}_{\text{ship}} = X^T_{\text{ship}} - X^0_{\text{ship}} = \overline{U_{\text{ship}}}T = \int_0^T U_{\text{ctd}}\, dt. \quad (2)$$

Here DX_{ship} can be inferred from the ships navigation

system (e.g., high accuracy GPS or other navigation data). Second, U_{ctd} is assumed to vary slowly in relation to the time between pings (dt). In particular one assumes that it is constant for each individual ADCP profile (the time it takes for the acoustic pulse to travel through the water ~0.2–0.5 s).

The U_{ocean} represents the unknown velocity profile of the ocean. The ocean velocity profile is divided into nz elements each representative over a depth range dz, thus

$$H = \mathrm{nz}dz. \tag{3}$$

Typically U_{ocean} is assumed to be constant over the duration of the cast (T) and any space–time variations will be interpreted as U_{noise}.

Finally, U_{adcp} represents the individual ADCP data that consist of nt velocity profiles. Each velocity profile consists of nbin velocity estimates. Note, that the number of useful velocity data (nbin) is strongly a function of instrumental parameter and ocean acoustic conditions.

The goal is to partition the observed ADCP velocities into the two signals (U_{ctd} and U_{ocean}). This can be done ''sequentially'' by considering some of the sampling aspects of the LADCP system. However, a more generic solution will be presented in section 5.

a. Shear and depth-averaged velocities

The U_{ocean} can be thought of as the sum of a depth average (barotropic) and depth varying (baroclinic) part:

$$U_{ocean}(z) = U_{ocean,barotropic} + U_{ocean,baroclinic}(z). \tag{4}$$

As we will show, LADCP data without external information such as ships position or bottom-track data can only constrain the baroclinic part of the ocean velocity.

The ADCP velocity profile (U_{adcp}) can also be thought of as the sum of two parts:

$$U_{adcp}(z) = U_{adcp,mean} + U_{adcp,variable}(z), \tag{5}$$

where $U_{adcp,mean}$ is a function of the CTD and ocean velocity. However, $U_{adcp,variable}$ and in particular its vertical derivative Us_{adcp}:

$$\mathrm{Us}_{adcp}(z) = \frac{\partial U_{adcp,variable}}{dz} \tag{6}$$

only depends on the shear of the ocean velocity and is *independent* of the CTD motion. This aspect of the LADCP system can be exploited to obtain a baroclinic ocean velocity profile ($U_{ocean,baroclinic}$).

The usual method to process LADCP data works as follows (e.g., Firing and Gordon 1990; Fischer and Visbeck 1993). First, the depth of the ADCP needs to be known. This can either be found by integrating the vertical velocity measured by the ADCP (Fig. 1):

$$z(t) = -\int_0^t w(t)\, dt, \tag{7}$$

or from a time series of CTD pressure. Next, the vertical shear is computed for each individual ADCP profile. Then all individual velocity shear estimates (Us_{adcp}) are averaged with respect to depth yielding an average top to bottom shear profile. Fischer and Visbeck (1993) discuss how careful shear data screening helps to improve the quality of the velocity profile. Finally, vertical integration of the shear profile results in a baroclinic ocean velocity profile ($U_{ocean,baroclinic}$).

Fischer and Visbeck (1993) also show how one recovers the barotropic ocean velocity ($U_{ocean,barotropic}$) by substituting the time integral of Eq. (4) into the time integral of Eq. (1):

$$\begin{aligned}\int_0^T U_{ocean,barotropic}\, dt &= \int_0^T U_{adcp}\, dt - \int_0^T U_{ctd}\, dt \\ &\quad - \int_0^T U_{ocean,baroclinic}\, dt - \int_0^T U_{noise}\, dt,\end{aligned} \tag{8}$$

which can be simplified by assuming that U_{noise} has no systematic biases and thus its time integral is small. Together with Eq. (2) we arrive at

$$\begin{aligned}U_{ocean,barotropic} &= \frac{1}{T}\left\{\int_0^T U_{adcp}\, dt - \int_0^T U_{ocean,baroclinic}[z_{ctd}(t)]\, dt\right\} \\ &\quad - U_{ship}.\end{aligned} \tag{9}$$

Such an equation can be written for each of the nbin time series of U_{adcp} (Fischer and Visbeck 1993).

Although U_{ctd} has not been used directly it can now be evaluated from Eq. (1) including the unknown error U_{noise}. In particular its time integral

$$\mathrm{DX}_{ctd}(t) = \int_0^t U_{ctd}(t')\, dt' \tag{10}$$

gives useful information about the relative position of the CTD package as a function of time (Fig. 1d).

Most LADCP software packages have more or less followed this shear-based processing scheme. A fundamental shortcoming is that one bad velocity bin will cause two bad shear estimates. Moreover, if the ranges are short, say nbin = 4, only two shear estimates can be found by using a central difference method. Finally, it is not obvious how to make use of extra information, such as surface ship drift, shipboard ADCP data, or bottom-referenced velocities to improve the estimated ocean velocity profile.

Before discussing an improved data processing approach we will review some of the fundamental LADCP sampling issues.

3. LADCP sampling

LADCP profiling is a compromise between range and resolution of individual ADCP velocity profiles versus their accuracy. The overall goal is obvious: *long range and high accuracy at fine vertical resolution.* However, it is less clear how particular choices impact the the accuracy of the final ocean velocity profile.

It seems helpful to define some fundamental nondimensional sampling ratios that can guide the LADCP user. It will become apparent that any hardware and parameter choices depend on the users requirements of resolution and accuracy of the resulting ocean velocity profile.

Today's ADCP vendors offer a range of instruments with different base frequencies, beam angles, and broad or narrow acoustic bandwidth. Without going into much detail the trade-offs are basically as follows: maximum range is obtained by low frequencies, small beam angles and a narrow bandwidth, while maximum accuracy requires exactly the opposite. There is no one obvious solution and several users favor range while others argue for accuracy. Even for a particular choice of hardware the user still can choose from a range of parameter settings. In the following we will discuss some of the consequences of these choices.

Most ADCPs can operate with different vertical resolutions, which is usually called the bin length (l_{bin}). The relevant parameter is actually the length of the acoustic pulse; however, most instruments set the pulse length equal or proportional to the bin length. Here it is assumed that the pulse length is equal to the bin length. The trade-off is between accuracy and resolution but also range. A long bin length has a higher accuracy and typically a larger range at the expense of vertical resolution. We will express the vertical resolution by a nondimensional number that compares the resolution of the ADCP (l_{bin}) to the desired resolution of the ocean velocity profile (dz):

$$R_{\text{res}} = \frac{dz}{l_{\text{bin}}}. \tag{11}$$

For most applications R_{res} will be chosen to be order one, which gives the highest possible accuracy for the desired final resolution.

One also needs to specify the time between pings (dt). Again there are trade-offs: long ranges prohibit a high ping rate and high ping rates use more energy and internal memory. We will express the ping rate in terms of a vertical sampling length (dl) that is defined as the product of the sampling interval (dt) and a typical lowering speed ($\overline{w}$):

$$dl = \overline{w}dt \sim \frac{2H}{\text{nt}}. \tag{12}$$

Here nt is the total number of ADCP profiles per cast and H is the depth of the desired velocity profile. The second nondimensional number compares this vertical sampling length scale to the desired resolution of the ocean velocity profile (dz):

$$R_{\text{samp}} = \frac{dz}{dl} = \frac{dz}{dt\overline{w}} = \frac{dz\text{nt}}{2H} = \frac{\text{nt}}{2\text{nz}}. \tag{13}$$

Typical values for R_{samp} are of order 10–50.

Finally, the ratio of the two compares the sampling length scale to the bin length:

$$R_{\text{ens}} = \frac{R_{\text{res}}}{R_{\text{samp}}} = \frac{dt\overline{w}}{l_{\text{bin}}}. \tag{14}$$

Here R_{ens} can guide the users decision about how many individual profiles (nens) he might want to internally average into one ensemble. The ensemble sampling rate can be expressed as $dt = dt_{\text{ens}} = \text{nens}dt_{\text{ping}}$. Solving for nens using Eq. (14) yields

$$\text{nens} = \frac{R_{\text{ens}}l_{\text{bin}}}{dt_{\text{ping}}\overline{w}}. \tag{15}$$

A conservative choice is to set R_{ens} to be one-third (three samples per sampling length). For example a lowering speed of $\overline{w} = 1$ m s^{-1}, a bin length of $l_{\text{bin}} = 10$ m, and a ping interval of $dt_{\text{ping}} = 1$ s yields nens ~ 3. Thus from a sampling point of view no significant information is lost if three pings are averaged together to what is called one ensemble.

If energy is not a factor one would choose to set the time between pings as small as possible without compromising the range. A large number of individual pings will improve ensemble accuracy by a factor of $(n)^{-1/2}$.

However, if the single ping accuracy is sufficient we would only need one velocity profile per vertical ADCP displacement of dz, the desired vertical resolution of the ocean velocity profile. Thus the maximum time between pings $dt_{\text{ping,max}}$ can be computed by setting R_{samp} to 1:

$$dt_{\text{ping,max}} = \frac{dz}{\overline{w}}. \tag{16}$$

In most applications the number of samples per vertical displacement dz is much lager than 1. Thus, one can begin the LADCP data processing with a data reduction stage: all profiles within the time it takes for the ADCP/CTD to cover a depth range dz can be averaged together. This will reduce the dataset typically by a factor of 10.

Note, that we have omitted the discussion of straightforward first-order quality control of the raw data to eliminate noise due to other acoustic sources, interference between instruments, reflections from moving targets (fish), and bottom returns from previous pings and the like. Many instruments have built-in quality controls, however, additional data screening is imperative to remove large outliers.

For a typical LADCP cast, where the down trace is followed by an up trace with possible stops to collect water samples, this yields nta = 2 dz ''super'' velocity

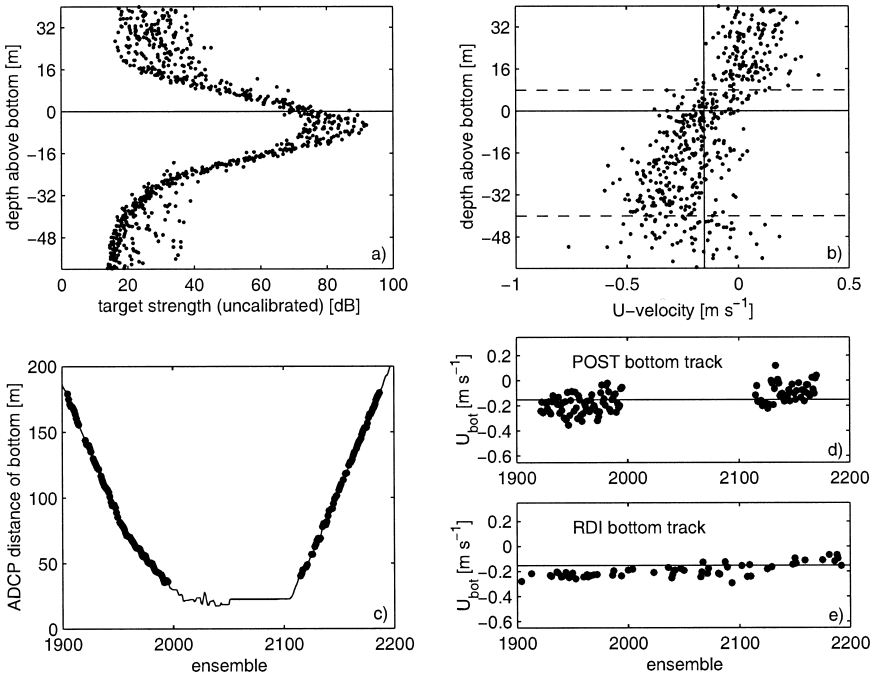

FIG. 2. An example of bottom tracking for a single LADCP cast using a broadband 150-kHz instrument. (a) Target strength as a function of depth above the bottom. The ADCP depth was computed using the standard procedure (see section 2) and a fixed bottom depth of 3475 m. (b) East–west velocity profiles as a function of depth above the bottom. Note, that velocities ''below'' the bottom (negative depths) are late arrivals and do not reflect the velocity below the seafloor. The vertical solid line represents the mean bottom U velocity averaged over the whole cast. The horizontal dashed lines represent the range from which data where used to calculate each individual post bottom-track velocity (3 bins centered 1 bin below the maximum target strength). (c) ADCP depth above bottom as a function of ensemble/time. The dots represents ensembles where post bottom-track velocities were estimated. (d) Time series of post bottom-track velocity as computed from the water velocity bins. (e) As (d) using the built-in bottom-track mode. (ADCP data courtesy B. King, IOS Southampton, United Kingdom.)

profiles (nz profiles for each trace). The resulting reduced dataset now has a sampling ratio (R_{samp}) of 1.

In summary, the nondimensional sampling parameter (R_{ens}, R_{samp}, and R_{res}) can help to describe the LADCP sampling with regards to the desired resolution of the final ocean velocity profile. We will revisit the sampling issue in the context of the problems dimension and final error discussion.

4. Bottom-referenced absolute velocities

The sea surface and ocean floor provide much larger backscatter compared to the oceans interior. Thus they can be detected from a large distance. As the LADCP approaches the bottom the strong reflections can be used to obtain a ''bottom velocity,'' which is essentially the motion of the instrument ($-U_{\text{ctd}}$) relative to the stationary bottom. This method is called bottom tracking and often used for shipboard ADCP applications to obtain absolute velocity profiles when the bottom is within the range of the instrument.

LADCP users have three options to obtain this valuable extra information. First, there is a dedicated bottom-track mode developed for shipboard ADCP applications (RDI-Primer 1989). A powerful and long (bottom track) pulse is inserted between the regular (water) pings from which a bottom velocity and range is calculated. From the choices available this is the most accurate method. However, it also requires significant extra power and in particular during deep casts only very few of those extra bottom-track pulses will give useful bottom velocities when the bottom is within the 20–300-m range of the ADCP.

Second, it is possible to diagnose the bottom velocity from the standard water pings. This postprocessing is possible if in addition to the velocity profiles the target strength (echo amplitude) was recorded. The postprocessing will be of a lesser quality for two reasons. First, the built-in bottom-track mode adjusts the pulse length in order to optimally sample the bottom. On average a longer pulse would have been used resulting in higher accuracy. Second, the backscattered signal is then analyzed at a much finer depth resolution compared to the typical bin length. The ''post'' method consists of a two-step process. First, the bin with maximum target strength is located and assigned to be the last bin above the

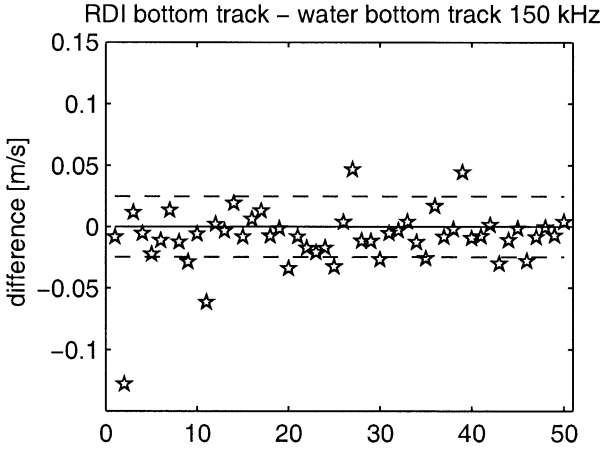

FIG. 3. Difference between the built-in RDI and the postprocessed bottom track using just the water bin data. Each symbols represent the cast averaged difference between either the u or v velocity components determined by the two methods for a total of 25 LADCP casts. Each cast contains typically 50–100 individual bottom-track estimates. The instrument used was a broadband RDI 150-kHz system (ADCP data courtesy of B. King, IOS Southampton, United Kingdom).

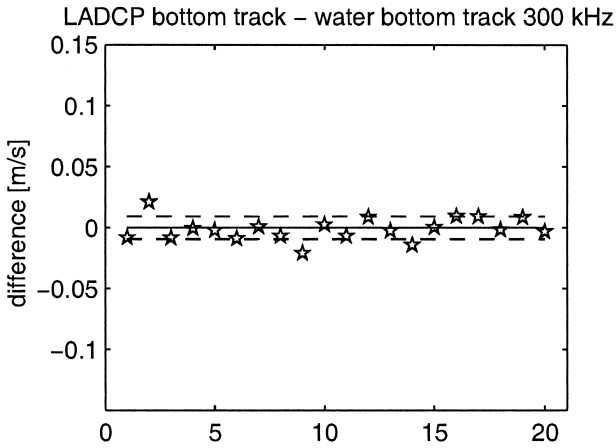

FIG. 4. Difference between the RDI LADCP and the postprocessed bottom track using just the water bin data. Each symbols represent the cast averaged difference between either the u or v velocity components determined by the two methods for a total of 10 LADCP casts. Each cast contains typically 50–100 individual bottom-track estimates.

bottom. Then, the median Doppler velocity taken from three bins centered around the bottom bin is interpreted as the desired bottom-track velocity ($-U_{\text{ctd}}$). Figure 2 shows an example for a 3500-m-deep LADCP cast. Note, that there is a small gradient within the three bins used to compute the post bottom track (Fig. 2b). As expected the scatter for each individual post bottom-track estimate is larger compared to the built-in RDI bottom track (Figs. 2d,e), however, the bias seems to be small.

More recently a very similar procedure has been included into the real-time LADCP processing for RDI workhorse ADCPs. This LADCP bottom-track option should be slightly more accurate compared to the post method since is uses a finer vertical resolution for the bottom track. However, it will not be quite as accurate as the full bottom-track mode since it uses the same (short) water track pulse instead of a dedicated longer ping. The internal LADCP bottom-track mode consumes no extra power and has marginal computational overhead and thus is highly recommended.

Figure 3 shows the difference between station-averaged pairs of bottom-track velocities determined from the RDI bottom-track (extra pulse) and the postprocessed method for 25 different stations. There is no significant mean difference and the scatter is within 2.5 cm s^{-1} (Fig. 3a).

Figure 4 shows the difference between the RDI-LADCP bottom track and the postprocessed bottom track using LADCP stations from the north-western Weddell Sea gyre. As expected both methods give similar results with an rms difference of about 1 cm s^{-1}.

In summary we have found little advantage in using the more accurate bottom-track mode and recommend using the new built-in LADCP bottom-track mode. If this is not an option one can always compute a sufficiently accurate bottom-track velocities if both the velocity and target strength raw data are recorded.

We have shown that when an LADCP station extends to the bottom valuable extra information about the motion of the CTD package can be extracted. Note, that all individual ADCP profiles with good bottom-referenced velocities can be used directly to obtain an average absolute velocity profile near the bottom. Those profiles themselves have scientific payoff for the study of bottom currents and abyssal flows (Gordon et al. 2001). They can also be compared to the lower part of the full-ocean LADCP profile. However, what should one do if they disagree?

In the next section we describe an advanced LADCP processing scheme that is able to incorporate bottom-referenced profiles and a range of other external information to improve the overall LADCP velocity profile.

5. A linear inverse method to process LADCP data

The fundamental equation (1) can be thought of as set of linear equations of the form:

$$\mathbf{d} = \mathbf{Gm} + \mathbf{n}, \tag{17}$$

where the vector $\mathbf{d}$ represents all ADCP velocities U_{adcp} from different depths within the water column. Here $\mathbf{n}$ represents the noise due to imperfect measurements ($\mathbf{d}$) and imperfect prediction of the true velocity field by $\mathbf{Gm}$. The unknown ocean velocity profile and the motion of the CTD package are combined into a single vector:

$$\mathbf{m} = \begin{bmatrix} m_{\text{ctd}} \\ m_{\text{ocean}} \end{bmatrix}, \tag{18}$$

which are related to the observations **d** by the model matrix **G**.

The dimension of the problem (i.e., the dimension of the matrix **G**) is defined by the number of velocity observations nd and the number of unknowns nm. The maximum number of observations is given by the number of velocity estimates per ping (nbin) times the number of profiles per cast (nt):

$$\text{nd} = (\text{nbin})(\text{nt}) = 2(\text{nbin})(\text{nz})R_{\text{samp}}. \tag{19}$$

If the profile extends to the bottom we typically lose ($\text{nd}_{\text{bottom}}$) velocity data:

$$\text{nd}_{\text{bottom}} = \frac{(\text{nbin}^2)l_{\text{bin}}}{\overline{w}dt} = (\text{nbin}^2)R_{\text{res}}R_{\text{samp}}. \tag{20}$$

However, in most cases the number of bottom-affected velocity is less than 10% of all data.

The unknowns are the sum of the ocean velocities plus the CTD velocities for each ensemble:

$$\text{nm} = \text{nm}_{\text{ctd}} + \text{nm}_{\text{ocean}} = \text{nz} + \text{nt}. \tag{21}$$

The number of ocean velocities is nz $= H/dz$ velocity elements of thickness dz. The vertical resolution of the ocean velocity profile (dz) can be chosen by the user but should not be much smaller than the bin length (see section 3, $R_{\text{res}} \geq 1$). The number of unknown CTD velocities is ($\text{nm}_{\text{ctd}} = \text{nt}$) equal to the number of pings. One can immediately see that the system is formally overdetermined if the ratio of known to unknown (F) is greater than 1 (assuming that all data are independent):

$$F = \frac{\text{nd}}{\text{nm}} = \frac{(\text{nbin})(\text{nt})}{\text{nz} + \text{nt}} = \frac{\text{nbin}}{\left(\dfrac{1}{2R_{\text{samp}}} + 1\right)}. \tag{22}$$

Obviously F depends on the sampling strategy. Let us imagine that the ADCP has a very high ping rate and the lowering speed of the CTD is very slow ($R_{\text{samp}} \gg 1$). The resulting number of ADCP profiles nt will be much larger than the number of desired ocean velocity data nz and $F \sim$ nbin. This shows that eventually the accuracy of the system is controlled by the number of (independent) vertical bins, that is, the ADCP instrument range.

In the limit of a rather high lowering speed and slow ADCP ping rate that still allows for useful sampling ($R_{\text{samp}} \sim 1$) gives only one ADCP profile for each desired ocean velocity depth cell. Thus nt is 2 times nz (1 U_{ctd} for each depth cell dz of the up and down cast). For this low sampling limit F approaches 2/3 nbin, which is not very different from the other limit. Thus LADCP systems with a range of more than two velocity bins (nbin > 2) are formally overdetermined.

a. A simple case

Let us consider a simple case to illustrate the set of linear equations (17). An ADCP is lowered with a constant vertical velocity to the bottom of the ocean and back to the surface (Fig. 1). The LADCP parameter are chosen such that $R_{\text{samp}} = R_{\text{res}} = 1$. The water depth is $H = 10\ dz$ and the range of the instrument is nbin $=$ 3. The instrument is looking toward the bottom. The number of unknown ocean velocities is nz $= 10$ and the total number of pings is nt $= 2(\text{nz})$ $R_{\text{samp}} = 20$. The number of water velocities is $\text{nd} - \text{nd}_{\text{bottom}} = \text{nbin}[\text{nt} - (\text{nbin})\ R_{\text{res}}\ R_{\text{samp}}] = 45$. Thus the system has nt + nz $= 30$ unknowns and 45 equations.

The array of linear equations (17) has the form

$$\mathbf{d} = \begin{bmatrix} u_{1,1} \\ u_{1,2} \\ u_{1,3} \\ u_{2,1} \\ \vdots \\ u_{3,1} \\ \vdots \\ u_{20,3} \end{bmatrix}, \qquad \mathbf{m} = \begin{bmatrix} u_{\text{ctd},1} \\ u_{\text{ctd},2} \\ u_{\text{ctd},3} \\ \vdots \\ u_{\text{ctd},20} \\ \text{—} \\ u_{\text{ocean},1} \\ u_{\text{ocean},2} \\ u_{\text{ocean},3} \\ \vdots \\ u_{\text{ocean},10} \end{bmatrix},$$

$$\mathbf{G} = \left[\begin{array}{ccccc|ccccc} 1 & 0 & 0 & \cdots & 0 & 1 & 0 & 0 & \cdots & 0 \\ 1 & 0 & 0 & \cdots & 0 & 0 & 1 & 0 & \cdots & 0 \\ 1 & 0 & 0 & \cdots & 0 & 0 & 0 & 1 & \cdots & 0 \\ 0 & 1 & 0 & \cdots & 0 & 0 & 1 & 0 & \cdots & 0 \\ \vdots & \vdots & \vdots & \ddots & \vdots & \vdots & \vdots & \vdots & \ddots & \vdots \\ 0 & 0 & 1 & \cdots & 0 & 0 & 0 & 1 & \cdots & 0 \\ \vdots & \vdots & \vdots & \ddots & \vdots & \vdots & \vdots & \vdots & \ddots & \vdots \\ 0 & 0 & 0 & \cdots & 1 & 0 & 1 & 0 & \cdots & 1 \end{array}\right]. \tag{23}$$

The full model matrix **G** is displayed in Fig. (5). Note that the model matrix is very sparse, which can be exploited to solve the problem efficiently. In the following we will discuss the least squares solution of a set of linear equations.

b. Interior solution

Equations of the form as show in (17) can be solved by least squares methods. One searches for solutions (**m**) that minimizes the squared difference between the data (**d**) and their prediction ($\mathbf{d}_{\text{pre}} = \mathbf{G}\mathbf{m}_{\text{est}}$). Solutions for overdetermined systems of linear equations are well known (e.g., Menke 1989):

$$\mathbf{m}_2^{\text{est}} = [\mathbf{G}^{\text{T}}\mathbf{G}]^{-1}\mathbf{G}^{\text{T}}\mathbf{d}, \quad \text{or} \tag{24}$$

$$\mathbf{m}_1^{\text{est}} = \mathbf{G}^{\text{T}}[\mathbf{G}\mathbf{G}^{\text{T}}]^{-1}\mathbf{d}, \tag{25}$$

where $\mathbf{m}_2^{\text{est}}$ represents the familiar least square solution

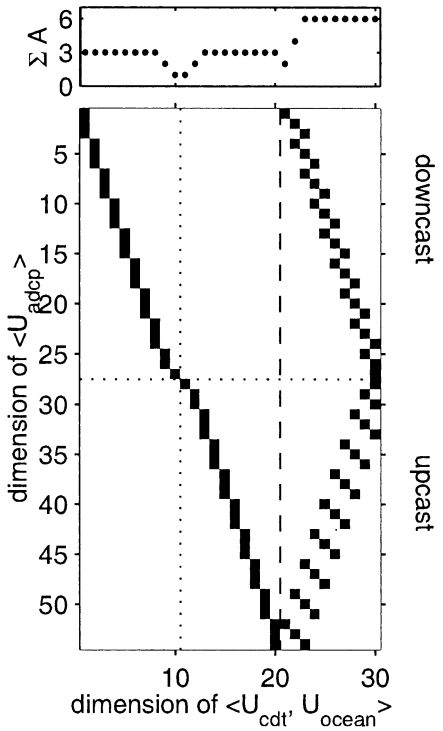

FIG. 5. Model matrix **G** for the simple test case. The observations are mapped to the unknown CTD motion (left) and to the ocean velocity (right). (top) The number of data points constraining each of the unkowns. On average there are nbin estimates for the CTD motion and 2 nbin estimates for each ocean velocity.

(L_2 norm) and $\mathbf{m}_1^{\text{est}}$ is a more robust estimator (L_1 norm) when noisy data are expected. The prediction error using the L_2 norm is given by $E = \Sigma_{i=1}^{N} (d_i - d_i^{\text{pre}})^2$ and for the L_1 norm is $E = [\Sigma_{i=1}^{N} |d_i - d_i^{\text{pre}}|]^2$.

Note that $\mathbf{GG}^{\text{T}}$ given by the simple case [Eq. (23) and Fig. 5] cannot be inverted because the unknowns (**m**) are not linear independent. This reflects the fact that LADCP data by themselves can only give the baroclinic ocean velocity profile without constraining the mean (see section 2). However, we can demand that the sum of all ocean velocities ($\Sigma\ \mathbf{m}_{\text{ocean}}$) be equal to zero:

$$\hat{\mathbf{d}} = \begin{bmatrix} \mathbf{d} \\ 0 \end{bmatrix};$$

$$\hat{\mathbf{G}} = \left[\begin{array}{cccc|cccc} & & \mathbf{G} & & & & & \\ 0 & 0 & 0 & \cdots & 0 & w & w & w & \cdots & w \end{array}\right]. \quad (26)$$

The magnitude of w controls how close the mean ocean velocity is expected to be to zero.

Now the problem is well posed and one can obtain an inverse solution. In some cases it might be helpful to weight each equation by its expected error. We had good success by using the size of the correlation velocity as a predictor for the relative quality of each velocity measurement. Note that we have purposefully chosen to multiply each observation [**d**(n)] and associated row of the model matrix (**G**) with their respective weight rather than applying a weight matrix during the solution. This allows us to use faster algorithm to find the solution. For example, we can solve

$$\mathbf{m}_{\text{chol}}^{\text{est}} = \text{backwardsub}[\mathbf{R}, \text{forwardsub}(\mathbf{R}^{\text{T}}, \mathbf{G}^{\text{T}}\mathbf{d})] \quad (27)$$

using

$$\mathbf{R} = \text{chol}(\mathbf{G}^{\text{T}}\mathbf{G}), \quad (28)$$

where chol denotes the Cholesky factorization:

$$\mathbf{A} = \text{chol}(\mathbf{B}), \quad \text{with } \mathbf{A}^{\text{T}}\mathbf{A} = \mathbf{B}. \quad (29)$$

The functions fowardsub and backwardsub solve lower- and upper-triangular sets of linear equations.

c. Barotropic constraint

One of the advantages of solving the LADCP problem using linear least squares methods is that additional information can easily be added to constrain the solution. For example, if good ship navigation exists we can prescribe the time average of the unknown package motion [U_{ctd}, Eq. (2)]. This will add one row to the equation array:

$$\hat{\mathbf{d}} = \begin{bmatrix} \mathbf{d} \\ wU_{\text{ship}} \end{bmatrix};$$

$$\hat{\mathbf{G}} = \left[\begin{array}{cccc|cccc} & & \mathbf{G} & & & & & \\ w\frac{\text{dt}_1}{T} & w\frac{\text{dt}_2}{T} & w\frac{\text{dt}_3}{T} & \cdots & w\frac{\text{dt}_{\text{nprof}}}{T} & 0 & 0 & 0 & \cdots & 0 \end{array}\right], \quad (30)$$

where dt_n denotes the time between subsequent package velocities (U_{ctd}) and w is a weight that controls how strong the solution is expected to obey this constraint. Note that this constraint should be used instead of Eq. (26).

d. Bottom track

It is also possible to include the bottom-referenced $U_{\text{cdt,bottom}}$ as a constraint. For each bottom-track velocity one equation can be added of the form

$$\hat{\mathbf{d}} = \begin{bmatrix} \mathbf{d} \\ wU_{\text{ctd,bottom}} \end{bmatrix};$$

$$\hat{\mathbf{G}} = \left[\begin{array}{cccc|cccc} & & \mathbf{G} & & & & & \\ 0 & 0 & w & \cdots & 0 & 0 & 0 & 0 & \cdots & 0 \end{array}\right]. \quad (31)$$

We can control the strength of the constraint by the weight w.

Alternatively one can add for each of the velocity

estimates where a bottom-referenced velocity exists a line of the form

$$\hat{\mathbf{d}} = \begin{bmatrix} \mathbf{d} \\ w(U_{\text{adcp}} - U_{\text{ctd,bottom}}) \end{bmatrix};$$

$$\hat{\mathbf{G}} = \left[\begin{array}{c} \mathbf{G} \\ \hline 0 \quad 0 \quad 0 \quad \cdots \quad 0 \,|\, 0 \quad 0 \quad w \quad \cdots \quad 0 \end{array}\right]. \tag{32}$$

Both forms are valid with slight differences in the error propagation.

e. Smoothness

In a similar matter we can demand that the estimated ocean velocity profile is smooth by adding a standard smoothness constraint:

$$\hat{\mathbf{d}} = \begin{bmatrix} \mathbf{d} \\ 0 \\ 0 \\ \vdots \\ 0 \end{bmatrix}; \qquad \hat{\mathbf{G}} = \left[\begin{array}{c|cccccc} & & & \mathbf{G} & & & \\ \hline 0 & \cdots & 0 & -1w & 2w & -1w & 0 \quad \cdots \quad 0 \\ 0 & \cdots & 0 & 0 & -1w & 2w & -1w \quad 0 \quad \cdots \quad 0 \\ \vdots & \ddots & \vdots & \vdots & \vdots & \vdots & \vdots \quad \ddots \quad \vdots \\ 0 & \cdots & 0 & 0 & 0 & 0 & 0 \quad \cdots \quad -1w \end{array}\right]. \tag{33}$$

The amount of smoothing of the ocean velocity profiles can be controlled by w.

By now it should be obvious how to add other constraints such as shipboard ADCP velocities, or any other external information.

f. Properties of the LADCP system

So far we have outlined how the LADCP problem can be written as a set of linear equations. We have shown how other constraints can be added to improve the estimated ocean velocity profile. The least squares framework also allows us to inspect how well the data constrain the solution. It is well known that the generalized inverse of the model matrix

$$\mathbf{G}_2^{-g} = [\mathbf{G}^{\mathrm{T}}\mathbf{G}]^{-1}\mathbf{G}^{\mathrm{T}}, \quad \text{or} \tag{34}$$

$$\mathbf{G}_1^{-g} = \mathbf{G}^{\mathrm{T}}[\mathbf{G}\mathbf{G}^{\mathrm{T}}]^{-1} \tag{35}$$

gives insights into the behavior of the solution. For example, Fig. 6 maps one row of the generalized inverse into the depth time space of LADCP sampling as a function of range of the ADCP. This illustrates how the observed ADCP velocities contribute to one of the ocean velocities at an intermediate depth (bin 13) for a problem that is similar to the sample case (section 5a), but with nz = 20. The right panels show the sum of the absolute weights as a function of depth. We find that the solution is more locally constrained for larger ranges (nbin). Also note, that the velocity bins close to the instrument and the ones far away contribute most to the solution. This is by no means optimal. We expect that the quality of the velocity estimates deteriorates with distance from the transducer. Appropriate weighting (see section 5a) with reduced confidence in the bins farther away from the ADCP will spread the influence more toward the middle bins.

We can also inspect the importance $\mathbf{n} = \text{diag}(\mathbf{N})$ of the data by inspecting the diagonal of the data resolution matrix:

$$\mathbf{N} = \mathbf{G}\mathbf{G}^{-g}. \tag{36}$$

Figure 7 plots the importance of the ADCP raw data for the sample case with nz = 20 for 3 different bin lengths. A short instrument range shows that the model will do a good job and fit every single data point well. Longer ranges will fit the individual data less well. However, the solution is then more robust against instrumental noise contained in the data. For many problems the importance of the data approaches the ratio of known to unknowns F^{-1}. Recall that our simple case had $R_{\text{samp}} = 1$ and hence $F = 3/2$ nbin [using Eq. (22)]. This typical value for $\mathbf{n}_{\text{typical}} = F^{-1} = 2/3(\text{nbin})$ is indicated by the dashed line. The best possible case with data covering the whole range of the ocean profile all the time (nbin = nz) will give an importance of $\mathbf{n}_{\text{opt}} = 3/2(\text{nz})$ as indicated by the dash–dotted line in Fig. 7.

A first guess for the error of the resulting velocity estimates can be obtained from the model parameter covariance matrix:

$$[\text{cov}(\mathbf{m}_2)] = \sigma_d^2[\mathbf{G}^{\mathrm{T}}\mathbf{G}]^{-1}, \quad \text{or} \tag{37}$$

$$[\text{cov}(\mathbf{m}_1)] = \sigma_d^2[\mathbf{G}\mathbf{G}^{\mathrm{T}}]^{-1}, \tag{38}$$

under the (not very realistic) assumption that all data are independent and of equal uncertainty given by σ_d^2. Figure 8 shows the diagonal of [cov (**m**)] for 3 different ranges (3, 5, and 7 bins) for a profile of a total depth of 20 bins. The smallest error for the ocean velocities is expected close to halfway between the bottom and the surface with increasing error toward the top and bottom.

Note that increased range reduces the mean error but more importantly the uncertainty at the top and bottom of the profile. Thus increased range will help to con-

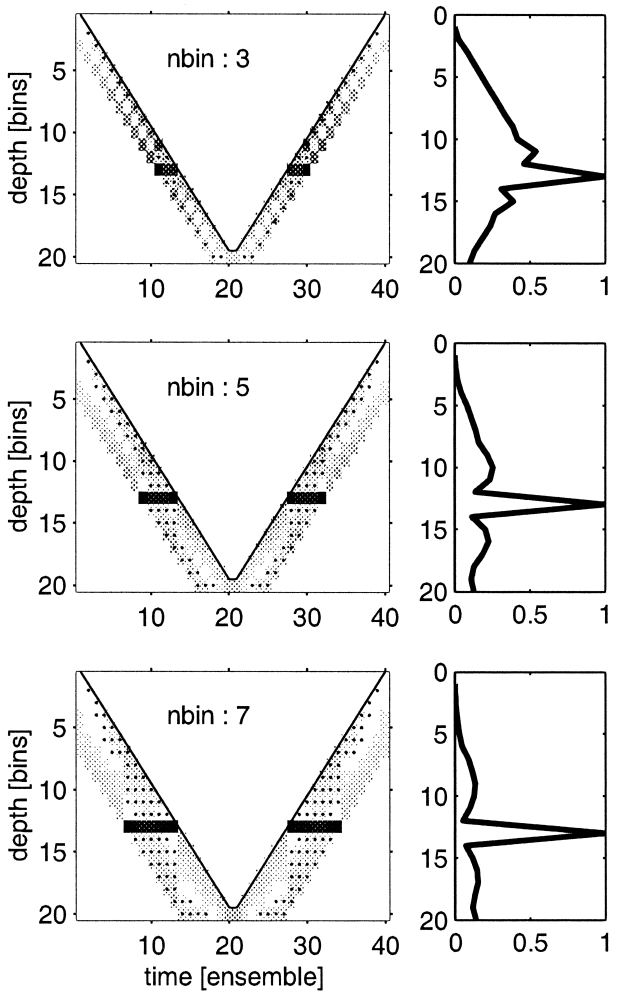

FIG. 6. Map of one row of the generalized inverse in the depth time plane. (top left) The sample case with a range of 3 bins, (middle left) 5, and (bottom left) 7 bins. Contributions are shaded with the darkest value corresponding to the maximum, negative contributions have an additional dot. The smaller panels on the right show the sum of the absolute weights as a function of depth. Note that the sums are normalized by their maximum value.

strain the low vertical modes of the ocean velocity profile.

Next we can explore the impact of bottom-referenced U_{ctd} data. Figure 9 shows the expected ocean and CTD velocity error for three scenarios. The top panel represents the estimated error for a solution that specifies the time mean U_{ctd} similar to Fig. 8. The next panel shows the expected velocity error when only bottom-

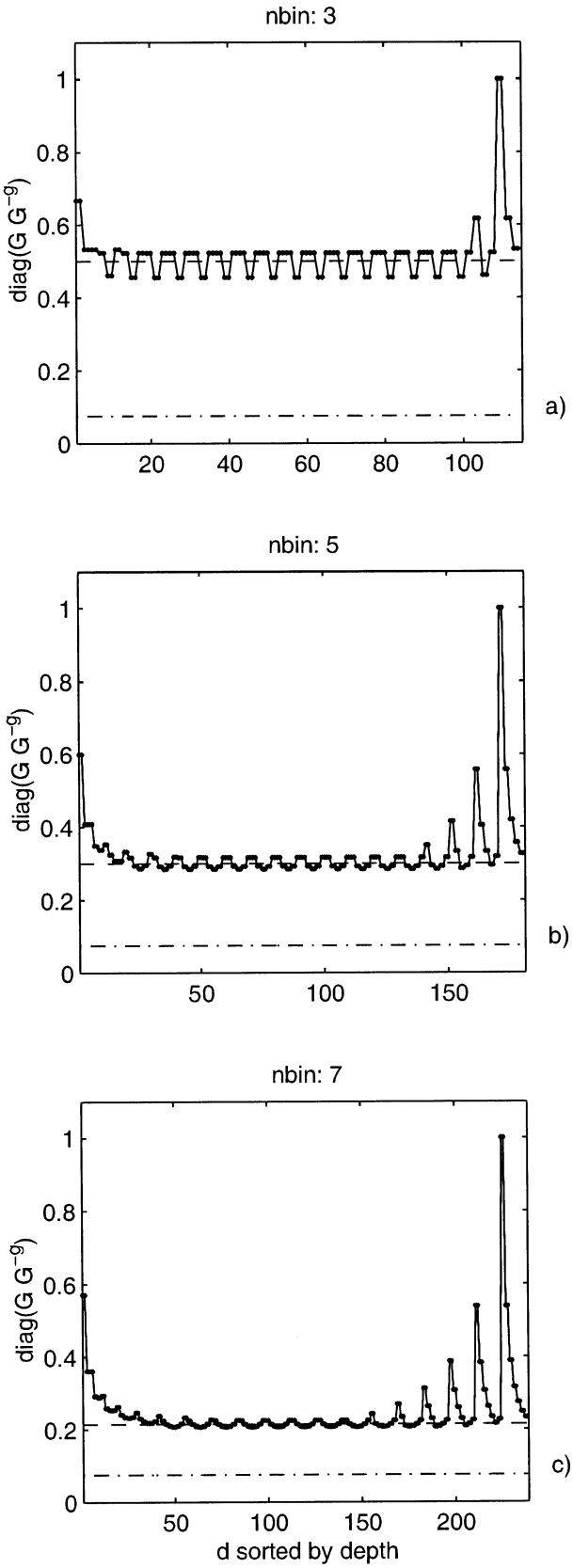

→

FIG. 7. Importance of the data [$\mathbf{n}$ = diag ($\mathbf{GG}^{-g}$)] is plotted vs the data vector. Note that the data vector has been sorted with regards to depth of the ADCP velocity data point. (a), (b), (c) The dependence of $\mathbf{n}$ as a function of instrument range nbin = 3, 5, and 7, respectively. The expected typical value for $\mathbf{n}$ is given by the dashed line and the best possible scenario by the dash–dotted line (see text for details).

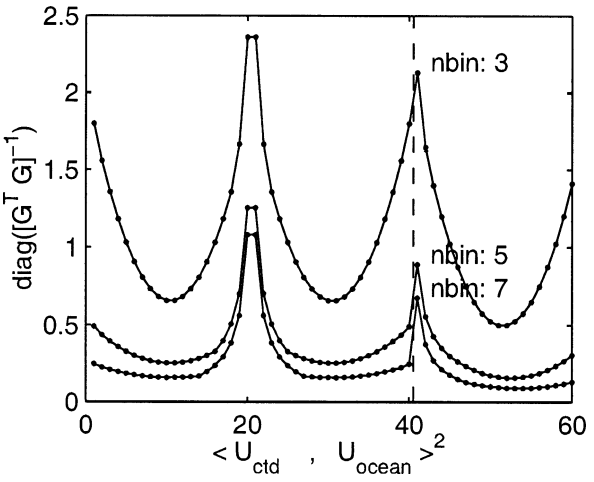

FIG. 8. Expected error of the model parameter [cov **m**] as a function of range (nbin). The vertical dashed line separates the estimated covariance for U_{ctd} from U_{ocean}.

track data are used to constrain the solution. Notice the low error near the bottom and the almost linear increase toward the surface. Finally, the bottom panels shows how the bottom track improves upon the standard case. The error is reduced at all depths with the most significant improvement near the bottom.

Finally, let us inspect how an error in the raw velocity data U_{adcp} effects the final velocity profile. The generalized inverse ($\mathbf{G}^{-g}$) maps the raw data onto the velocities. Figure 10 shows how a spike in the data influences the final velocities $m'_{\text{est}} = \mathbf{G}^{-g}\mathbf{d}'$. Two different cases of $\mathbf{d}'$ are chosen. The left column shows how a spike in the middle of one ADCP profile (n_{spike} = nbin/2) affects the solution for different values of the instrument range. The left column contrasts that with a spike at the end of one ADCP profile (n_{spike} = nbin). One can clearly see that noisy data at the beginning and/or end of individual ADCP profiles can introduce jumps in the resulting ocean velocity profile. In particular systems with short ranges are very sensitive to such noise.

We conclude that expressing the LADCP system in terms of an array of linear equations allows us to gain valuable insight into the propagation of errors through the system.

6. Summary and discussion

Two aspects of LADCP velocity profiling have been discussed: information obtained from bottom-track data and an improved data processing method using a linear

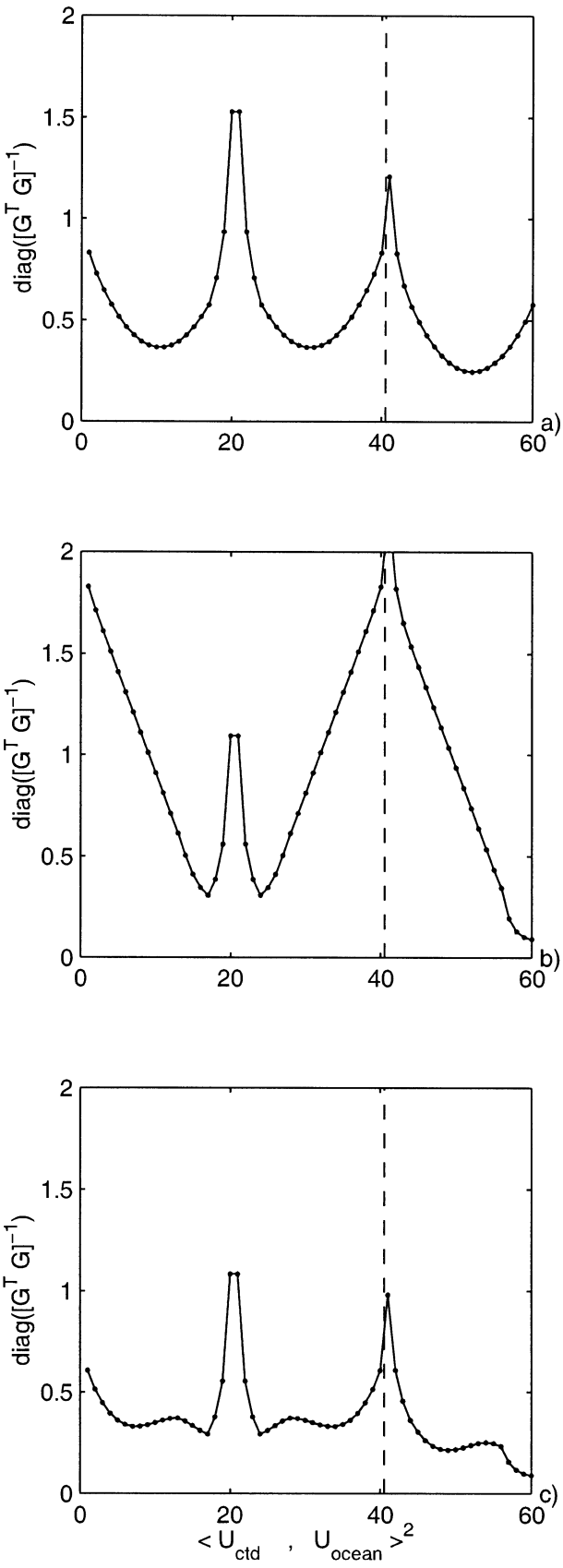

FIG. 9. Expected error of the model parameter for a LADCP simulation with nz = 20 and nbin = 4. (a) A solution that is constrained by specifying the time mean U_{ctd}. (b) Only bottom-track data in addition to the standard water velocities are used. (c) The bottom-track and time mean U_{ctd} constraints are used.

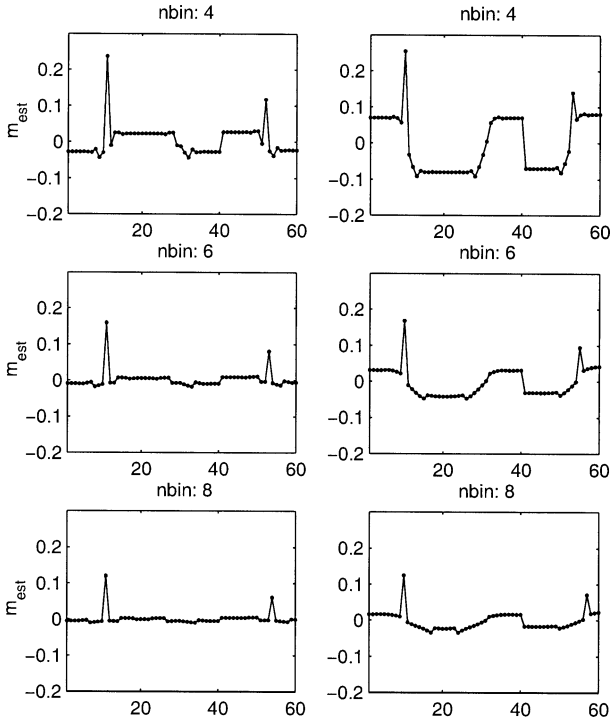

FIG. 10. Impact of a single spike in the ADCP velocity data on the solution as a function of range (nbin). (left column) The influence of a spike in the middle of one ADCP profile, and (right column) representation of how a spike at the end influences the model parameter estimates. All cases are for nz = 20 with variable range (top to bottom) nbin = 3, 5, and 7.

least squares method. A subset of commercially available ADCPs can be lowered down to a depth of 6000 m and allows us to obtain top to bottom velocity profiles in most parts of the world's oceans. When ADCPs approach the bottom they are also capable to determine a bottom-referenced velocity that is directly measuring the motion of the instrument. This additional information can be used to interpret the lower part of an LADCP profile as absolute velocities. We have shown that instead of the extra bottom-track pulse, the bottom-referenced velocity can be obtained by postprocessing the standard water bins. A comparison between the two methods gave encouraging agreement.

However, what was less obvious is how to use this extra information to improve the overall quality of the final ocean velocity profiles. The main thrust of the paper is to outline the details of an improved data processing scheme that recasts the LADCP problem as a set of linear equations that can be solved using standard least squares methods. One of the great advantages of this approach is that it is very straightforward to include additional constraints such as bottom-referenced velocities, smoothness of the solution, and other aspects of the LADCP system. Moreover, solutions to linear equations are well understood and fundamental aspects of the LADCP system can be deduced. We have shown that increasing the range has the largest effect in order to reduce the overall error of the system. However, it also becomes clear, that noise in the first or last bins of each individual profile introduce large uncertainties on the final solution.

In the following we will summarize the important findings of this paper by reviewing step by step the processing of one LADCP station.

LADCP data processing

We will use a station taken at 58°43′S and 44°30′W just north of the Weddell Sea in the Southern Ocean obtained on board *Palmer* as part of the DOVETAIL project in August 1997 (Gordon et al. 2001). The ADCP hardware used were two RDI workhorse LADCP systems that are pressure rated for ocean depths up to 6000 m. The bin length of the 300 kHz units was set to $l_{\text{bin}} = 16$ m and the time between pings was 0.6 s. In order to save internal memory we averaged three successive profiles together to one ensemble. At this station the water depth was about 2100 m and approximately nt = 3400 velocity profiles (ensemble) were taken within 2.5 h. The two ADCPs were mounted on the CTD frame one looking upward and the other one looking downward to maximize the total range of velocity observations. Throughout most of the cast, each instrument had a range of 160 m or approximately nbin = 9. Thus the total number of individual raw ADCP velocities is ~30 000 for each instrument. The instruments were connected to each other and one was designated the master and the other the slave. The slave listens to the master for the ping command and both units ping simultaneously. Thus the dimension of the problem is about 60 000 known raw data, 3400 unknown CTD velocities, and 100 unknown ocean velocities with 20-m vertical resolution. A brute force inversion of the problem would require the inversion of a 60 000 by 3500 complex element matrix that alone will take up more than 100 MB of memory and several tens of minutes of CPU time on a 500 MHz Pentium III processor. Note that extrapolating this to a 6000-m-deep profile with single pings each 0.5 s could easily yield 100 000 unknowns, which would be impractical to invert on the current generations of notebook computers. Thus a more clever treatment of the problem is advisable.

The vertical resolution of our problem is of order 1 [R_{res} 1, Eq. (11)] as it should be. However, the sampling resolution [R_{samp}, Eq. (13)] is 12. This suggests that after some first-order raw data screening the number of ensembles can be significantly reduced. We have chosen to average all ADCP velocity data together as long as the CTD is within a 20-m vertical bin. This reduces the number of ensembles from 3400 to 190 and now R_{samp} is about 1.

The LADCP bottom-track mode detected 390 bottom reflections ranging between 40 and 220 m off the bottom. The bottom-track data were averaged in the same

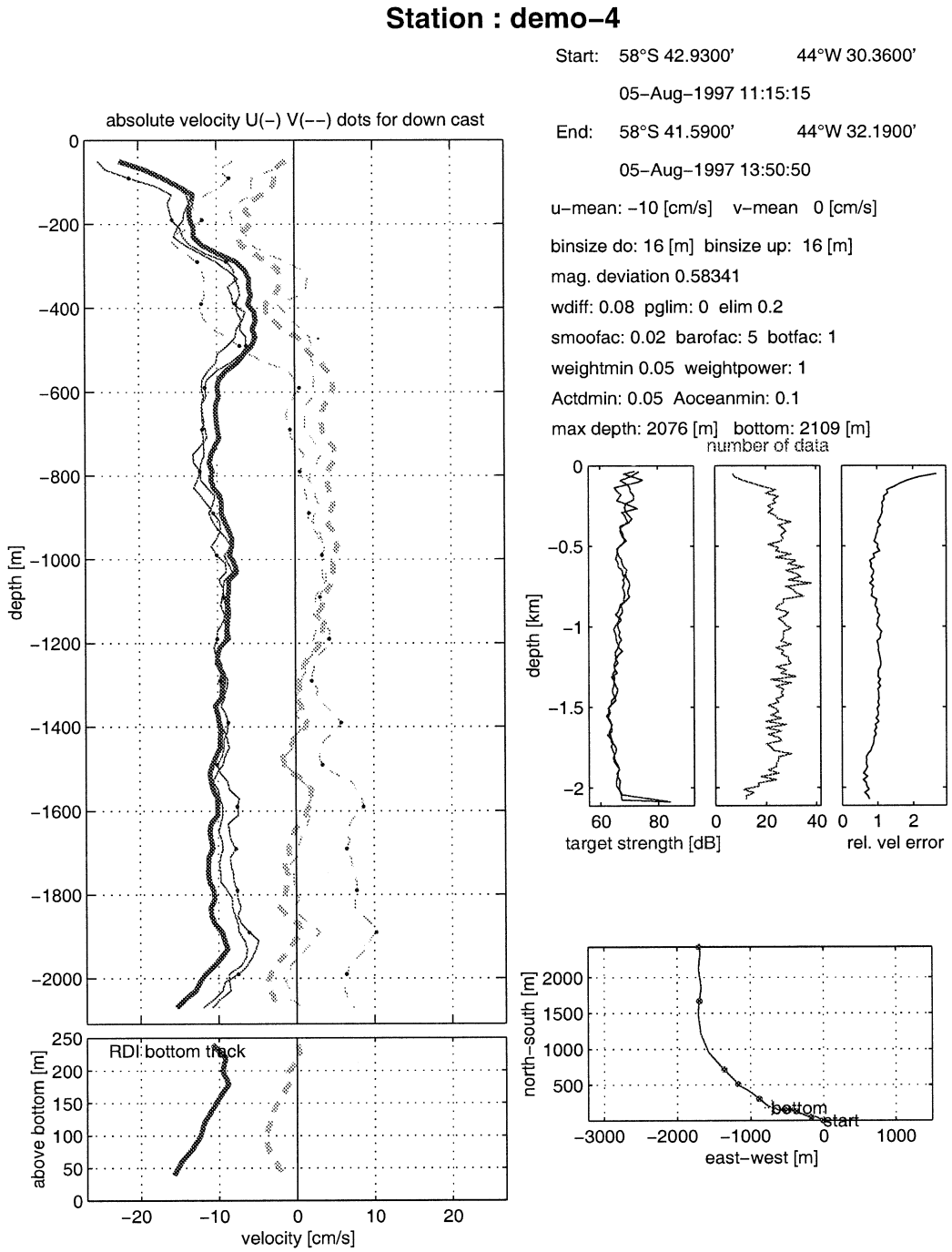

FIG. 11. Screen shot of the LADCP data processing software output.

way as the water velocity data resulting in 15 average bottom-track data. All profiles that have bottom-track information were used to obtain a bottom-referenced velocity profile by solving a set of inverse equations similar to Eqs. (17) and (23), where the data are $U_{\text{adcp}} - U_{\text{adcp,bottom}}$. The model matrix $\mathbf{G}_{\text{bottom}}$ directly maps $U_{\text{ocean,bottom}}$ to the data since the CTD/ADCP velocity is known.

The full depth velocity problem had 2810 equations including the barotropic constraint, the bottom track, and smoothing of the ocean velocity profile to estimate 271 unknowns. The inverse solution plus some of the formal errors was found within 3 s of CPU time. The whole station was processed in less than 1 min including reading of the raw data, finding the depth of each ping, raw data screening, reducing the data, preparing for the

inverse solution, solving it, and plotting and saving the results to disk. An illustration of the final ocean velocity for the particular station is given in Fig. 11. Three velocity profiles are shown for each of the components: The solid line is the best estimate including the ships navigation and bottom-track constraint. The two thin lines are solutions based in the down and up cast alone (excluding the bottom track). Their vertical mean was set to be equal to the respective full velocity solution. One can see, that inclusion of the bottom track can force the best guess to be outside of the envelope defined by the down and up cast. Note also, that the relative velocity error plot shows that the most uncertain velocity estimate is close to the surface.

We conclude that solving the LADCP system as a set of linear equations is feasible with today's powerful personal computers.

Acknowledgments. This work has benefited from numerous interactions amongst the LADCP user group (http://www.ldeo.columbia.edu/~visbeck/ladcp) in particular Juergen Fischer, Christian Mertens, Gerd Krahmann, Bruce Huber, Lee Gordon, Brian King, and Dan Torres. Brian King has kindly provided some bottom-track LADCP profiles. The first version of the manuscript was prepared during a 3-month-long visit at CSIRO, Hobart (winter 1998/99). I am in debt to Trevor McDougall for his hospitality and stimulating discussions as well as to Peter MacIntosh for providing me with a fast MATLAB based solver for linear equations. Two anonymous reviewers provided helpful suggestions that improved the manuscript.

REFERENCES

Beal, L., and H. Bryden, 1997: Observations of an Agulhas undercurrent. *Deep-Sea Res.,* **44,** 1715–1724.

Firing, E., 1998: Lowered ADCP developments and use in WOCE. *WOCE Newsletter,* No. 30, WOCE International Project Office, Southampton, United Kingdom, 10–13.

——, and R. Gordon, 1990: Deep ocean acoustic Doppler current profiling. *Proc. IEEE Fourth Working Conf. on Current Measurements,* Clinton, MD, IEEE, 192–201.

——, S. E. Wijffels, and P. Hacker, 1998: Equatorial subthermocline currents across the Pacific. *J. Geophys. Res.,* **103,** 21 413–21 423.

Fischer, J., and M. Visbeck, 1993: Deep velocity profiling with self-contained ADCPs. *J. Atmos. Oceanic Technol.,* **10,** 764–773.

——, F. Schott, and L. Stramma, 1996: Currents and transports of the Great Whirl-Socotra Gyre system during the summer monsoon, August 1993. *J. Geophys. Res.,* **101** (C2), 3573–3588.

Gordon, A., M. Visbeck, and B. Huber, 2001: Export of Weddell Sea deep and bottom water. *J. Geophys. Res.,* **106,** 9005–9017.

Hinrichsen, H., and A. Lehmann, 1995: A comparison of geostrophic velocities and profiling ADCP measurements in the Iberian Basin. *J. Atmos. Oceanic Technol.,* **12,** 901–914.

Joyce, T., T. Bitterman, and K. Prada, 1982: Shipboard acoustic profiling of upper ocean currents. *Deep-Sea Res.,* **29,** 903–913.

Menke, W., 1989: *Geophysical Data Analysis: Discrete Inverse Theory.* Academic Press, 289 pp.

RDI-Primer, 1989: Acoustic Doppler current profilers principles of operation: A practical primer. RDI Instruments, 54 pp.

Schott, F., J. Fischer, J. Reppin, and U. Send, 1993: On mean and seasonal currents and transports at the western boundary of the equatorial Atlantic. *J. Geophys. Res.,* **98,** 14 353–14 368.

Spain, P. F., D. L. Dorson, and H. T. Rossby, 1981: Pegasus: A simple, acoustically tracked velocity profiler. *Deep-Sea Res.,* **28A,** 1553–1567.

Stramma, L., J. Fischer, and F. Schott, 1996: The flow field off southwest India at 8°N during the southwest monsoon of August 1993. *J. Mar. Res.,* **54,** 55–72.

Wijffels, S. E., M. M. Hall, T. Joyce, D. J. Torres, P. Hacker, and E. Firing, 1998: Multiple deep gyres of the western North Pacific: A WOCE section along 149°E. *J. Geophys. Res.,* **103,** 12 985–13 009.

Wilson, W., 1994: Deep ocean current profiling with a Broadband Acoustic Doppler Current Profiler. *Proc. Oceans '94,* New York, NY, Institute of Electrical and Electronics Engineers, 660–665.

——, and W. E. Johns, 1997: Velocity structure and transport in the Windward Island Passages. *Deep-Sea Res.,* **44,** 487–520.